

High-spin states above the isomers in neutron-rich iodine nuclei near $N = 82$

R. Banik,^{1,2,*} S. Bhattacharyya,^{1,2,†} M. Rejmund,³ A. Lemasson,³ S. Biswas,³ A. Navin,³ Y. H. Kim,^{3,‡} C. Michelagnoli,^{3,‡} I. Stefan,⁴ P. Bednarczyk,⁵ Soumik Bhattacharya,^{1,2} E. Clément,³ H. L. Crawford,⁶ G. de France,³ P. Fallon,⁶ G. Frémont,³ J. Goupil,³ B. Jacquot,³ H. J. Li,³ J. Ljungvall,⁷ A. Maj,⁵ L. Ménager,³ V. Morel,³ G. Mukherjee,^{1,2} R. Palit,⁸ R. M. Pérez-Vidal,⁹ J. Ropert,³ and C. Schmitt³

¹Variable Energy Cyclotron Centre, 1/AF Bidhannagar, Kolkata 700064, India

²Homi Bhabha National Institute, Training School Complex, Anushaktinagar, Mumbai 400094, India

³GANIL, CEA/DRF-CNRS/IN2P3, Boulevard Henri Becquerel, BP 55027, F-14076 Caen Cedex 5, France

⁴Institut de Physique Nucleaire, IN2P3-CNRS, Université Paris Sud, Université Paris Saclay, 91406 Orsay Cedex, France

⁵Institute of Nuclear Physics PAN, 31-342 Kraków, Poland

⁶Nuclear Science Division, Lawrence Berkeley National Laboratory, Berkeley, California 94720, USA

⁷CSNSM, Université Paris-Sud, CNRS/IN2P3, Université Paris-Saclay, 91405 Orsay, France

⁸Department of Nuclear and Atomic Physics, Tata Institute of Fundamental Research, Mumbai, 400005, India

⁹Instituto de Física Corpuscular, CSIC–Universitat de València, E-46980 València, Spain



(Received 13 May 2020; accepted 9 October 2020; published 29 October 2020)

Excited states of neutron-rich iodine isotopes $^{130-134}\text{I}$ above the high-spin isomers have been identified using prompt-delayed γ -ray spectroscopy. The iodine isotopes were produced as fission fragments of fusion-fission and transfer induced fission of $^9\text{Be}(^{238}\text{U}, f)$ at a beam energy of 6.2 MeV/u. The complete (A, Z) identification was obtained using the large acceptance magnetic spectrometer VAMOS++. The AGATA γ -ray tracking array was used to detect the prompt γ rays while the delayed γ rays (in the time range of 100 ns to 200 μs) from the isomeric states were identified by the EXOGAM segmented clover detectors, placed behind the focal plane of the VAMOS++ spectrometer. The high-spin states above the (8^-) isomers in $^{130,132}\text{I}$ were populated for the first time, and a new isomer in ^{132}I was identified. A new γ -ray transition was also assigned to the level structure of ^{134}I . Prompt transitions above the $19/2^-$ isomer were identified in $^{131,133}\text{I}$, for the first time. The level structures are interpreted in terms of the systematics of odd- Z nuclei above the $Z = 50$ shell closure and large-scale shell model calculations.

DOI: [10.1103/PhysRevC.102.044329](https://doi.org/10.1103/PhysRevC.102.044329)

I. INTRODUCTION

Nuclei with either odd numbers of valence protons (odd- Z) or odd numbers of valence neutrons (odd- N) near a major shell closure have always been of special interests, as their level structures carry an important link to nucleon-nucleon effective interaction [1–3]. The doubly magic ^{132}Sn ($Z = 50$, $N = 82$) has a robust shell closure, having its first excited state at 4.0 MeV [4]. Thus, the single-particle excitations, particle-hole interactions, and mixing of various single-particle configurations in nuclei with few valence particles or holes around ^{132}Sn have been the subject of contemporary interest, both experimentally [5–9] and theoretically [2,10]. In particular, nuclei with a few odd valence protons outside the $Z = 50$ shell with a few neutron holes in the $N = 82$ shell provide important information about the multiplets of

various particle-hole configurations. The excited states of these nuclei also provide key inputs in understanding the effective interactions used for large-scale shell model calculations. The presence of the high- j , unique parity $h_{11/2}$ orbital in the $Z, N = 50$ –82 shell, for both protons and neutrons, plays the major role in generating the high-spin states for nuclei in the $A = 130$ region. Configurations involving $h_{11/2}$ neutron holes are also responsible for systematic occurrence of isomers in odd- A as well as in odd-odd nuclei in this region. It would be thus interesting to investigate the level structure above these isomers to understand the involvement of the $h_{11/2}$ orbital and relative contributions of proton and neutron occupancies in this high- j orbital in generating the high-spin states above the isomers.

The iodine ($Z = 53$) isotopes with three protons outside $Z = 50$ and a few neutron holes or particles in the vicinity of the $N = 82$ have attracted attention of several recent studies. The importance of several structures based on $\pi g_{7/2}$, $\pi d_{5/2}$, and $\nu h_{11/2}$ orbitals has been reported systematically in odd-odd iodine isotopes up to $N = 75$ [11–14]. In odd- A iodine isotopes $^{127,129}\text{I}$, collective bands based on $\pi g_{7/2}$, $\pi d_{5/2}$, and $\pi h_{11/2}$ configurations have been reported. At higher spins, the states associated with a neutron pair breaking, involving

*Present address: Institute of Engineering and Management, Saltlake Sector V, Kolkata 700091, India.

†Corresponding author: sarmi@vecc.gov.in

‡Present address: Institut Laue-Langevin, F-38042 Grenoble Cedex, France.

orbitals $\pi g_{7/2}$ and $\nu h_{11/2}$, have also been observed [15,16]. Towards the $N = 82$, isomeric states ($19/2^-$ and $23/2^+$) dominated by two neutron-hole configurations coupled to the odd number of protons have been identified in $^{131,133}\text{I}$ ($N = 78, 80$) [17].

The spectroscopic information on high-spin states above the isomers of neutron-rich iodine isotopes in the $A \approx 130$ mass region, towards $N = 82$, is very limited. This is mainly because of the fact that these nuclei are at the limit of accessibility using fusion evaporation reactions, which can be used to produce the isotopes up to ^{129}I . For heavier isotopes, either multi-nucleon transfer reactions [17] or spontaneous fission of ^{252}Cf [18] or ^{248}Cm [19–21] are used to study the high-spin excitations. Studies of the spontaneous fission of actinides utilize the prompt high-fold γ - γ coincidence technique to identify the high-spin states. With this technique, it is not possible to obtain γ - γ correlations across long-lived isomers. In these experiments, neutron-rich iodine nuclei, above the $N = 82$ shell closure, can be studied [20–23]. In contrast, for neutron-rich iodine isotopes $^{130,132}\text{I}$, just below $N = 82$, almost no information on high-spin states is available. Low lying long lived high-spin isomers, (6^-), (8^-), have been identified systematically in odd-odd neutron-rich iodine isotopes. Few states above the (8^-) isomer ($T_{1/2} = 3.52$ min) in ^{134}I [18] have been identified, but no excited states above the corresponding (8^-) isomers in ^{132}I ($T_{1/2} = 1.38$ h) and in ^{130}I ($T_{1/2} = 315$ ns) were reported.

In the present work, the neutron-rich iodine isotopes $^{130-134}\text{I}$ were produced as fission fragments and their excited states were characterized from in-beam prompt-delayed γ -ray spectroscopy after isotopic identification (A, Z). The high-spin excitations above the (8^-) isomer and the corresponding γ -ray transitions in odd-odd iodine nuclei $^{130,132}\text{I}$ were observed for the first time. A new isomer in ^{132}I was identified and the half-life was measured from the corresponding γ -ray decay. New prompt γ -ray transitions above the isomeric states in $^{131,133}\text{I}$ and ^{134}I were also identified. Using large-scale shell model calculations, the contribution of the neutron hole occupancy of the $\nu h_{11/2}$ orbital to the high-spin negative parity states is analyzed.

II. EXPERIMENT AND DATA ANALYSIS

The excited states of neutron-rich iodine isotopes were populated via fusion-fission and transfer induced fission reactions in inverse kinematics, using a ^{238}U beam of energy 6.2 MeV/u bombarding ^9Be targets of thickness 1.6 and 5 μm at Grand Accélérateur National d'Ions Lourds (GANIL). The isotopic identification (A, Z) of the fission fragments was obtained using the large acceptance magnetic spectrometer VAMOS++, placed at an angle of 20° with respect to the beam axis [24–28]. The Z identification was obtained by ΔE - E measurement using the ionization chamber placed at the focal plane of VAMOS++. Time of flight of each fragment was measured using a dual position-sensitive multiwire proportional counter (DPS-MWPC) [27] placed at the entrance of VAMOS++ and a MWPC placed at the focal plane. The focal plane detector system also consisted of two drift chambers (DC) for tracking. The mass number (A), atomic

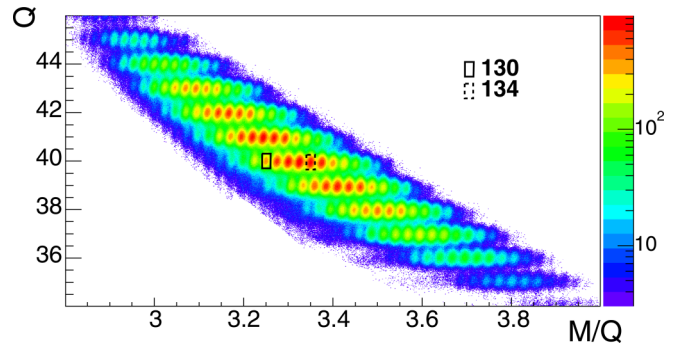


FIG. 1. Charge state (Q) as a function of the mass over charge (M/Q) after the selection of iodine ($Z = 53$). The iodine isotopes are obtained from various charge states and the identification of $A = 130$ and 134 are marked for charge state $Q = 40$.

number (Z), atomic charge (Q), and the velocity vector of the fission fragments were determined on an event-by-event basis. The (M/Q) parameter was obtained from the reconstructed magnetic rigidity ($B\rho$) and velocity of the fragment. The resolutions (FWHM) achieved for Z , A , and Q are 1.3%, 0.4%, and 1.3% respectively. The nuclei were identified individually following their Z (ΔE - E), A and Q (Q - M/Q) selection. The narrow gates were applied to obtain the corresponding γ -ray spectra. The identification of iodine isotopes obtained from the two-dimensional plot of Q and M/Q is shown in Fig. 1. Further details and identification spectra are given in Ref. [28]. The possible contaminations of the γ -ray spectra by the nuclei associated with the neighboring Z , A , and Q were individually examined. The analysis of the corresponding γ -ray spectra allowed us to evaluate any possible small contamination and perform the suitable background subtraction case by case.

The prompt γ rays (γ_p) emitted from the recoiling fission products at the target position were detected using position sensitive γ -ray tracking array AGATA [29]. In the current experimental setup, AGATA consisted of 32 crystals and was placed 13.5 cm away from the target. As the nuclei fly away from the target, the AGATA array does not detect γ rays emitted after a few ns. No lifetime information was extracted using the γ rays detected in AGATA. The data were acquired under the condition of a coincidence between the prompt γ rays and DPS-MWPC within 300 ns. The typical time of flight for the iodine isopes in VAMOS++ was ≈ 200 ns. An array of seven EXOGAM segmented clover detectors [30] was also placed behind the ionization chamber of VAMOS++ in a wall configuration to detect the delayed γ rays (γ_D). The trigger for detecting the delayed γ rays detected at EXOGAM detectors was generated when a delayed γ -ray followed the prompt trigger within 200 μs . The time between the ion implantation and the delayed γ -ray event was measured using time-stamp differences obtained using a 100 MHz clock. The time resolution of EXOGAM detectors was ≈ 6 ns at 1 MeV. The decay curves were obtained from the time difference between the signals from the DPS-MWPC placed at the entrance of VAMOS++ and the EXOGAM detectors placed at the focal plane, and thus the time measured is independent of the time

of flight. Due to the use of logic delays in the trigger, the time (t_{Decay}) has 800 ns offset, thus the true reaction time corresponds to a $t_{\text{Decay}} = 800$ ns. The shortest lifetimes measured in the focal plane using the present experimental setup are $T_{1/2} = 60(20)$ ns and $90(16)$ ns in ^{126}Sb [31]. Further details of the experimental setup consisting VAMOS++, AGATA and EXOGAM can be found in Ref. [28].

Coincidence matrices were constructed between prompt γ rays (γ_P - γ_P), prompt-delayed γ rays (γ_P - γ_D), and any two delayed γ rays (γ_D - γ_D) [28]. Also, small corrections for isobaric and isotopic contamination (if any) were taken into account for each of the iodine isotopes in both prompt and delayed spectra following the procedure described in Ref. [28]. Intensity determination and corrections for half-life calculations have also been carried out, as described in Ref. [28]. The spin-parities of the excited states were tentatively assigned based on systematics of iodine isotopes and shell-model calculations.

III. RESULTS

A. ^{130}I

Prior to the present study, the spectroscopic information of ^{130}I was investigated via (n, γ), (d, p) reactions using two Ge(Li) detectors [32] and also via the ($^3\text{He}, t$) reaction [33]. Half-lives of four isomeric states at 39.95 keV (8.3 ± 1.0 min), 69.58 keV (133 ± 7 ns), 82.39 keV (315 ± 15 ns), and 85.10 keV (254 ± 4 ns) were also reported in Ref. [32] with probable spin-parity assignments of (2^+), (6^-), (8^-), and (6^-) respectively. The 82.39 keV level was assigned as (8^-) in Ref. [32], though this assignment for the 82.39 keV level was not adopted in Ref. [34]. No high-spin states above the (6^-) or (8^-) isomers have been reported for ^{130}I prior to the present work.

Prompt-delayed spectroscopy of isotopically identified fission fragment gives the unique opportunity to investigate the high-spin excited states of this isotope above the isomers. Figure 2 shows the proposed level scheme of ^{130}I , obtained from the present work. All the transitions placed in the level scheme above the isomeric state were observed for the first time and are marked in red. The relative placements of these γ -ray transitions in the level scheme were done based on their mutual coincidence relationships and relative intensities. The details of the γ rays of ^{130}I with tentative spin and parity of the initial (J_i^π) and the final (J_f^π) states are given in Table I. Fig. 3(a) shows the prompt singles γ -ray spectrum (γ_P) after Doppler correction, in coincidence with the ^{130}I fragments. A coincidence spectrum corresponding to the sum of gates on 748, 922, and 971 keV transitions is shown in Fig. 3(b). The 748, 922, 135, and 971 keV γ rays were found to be in mutual coincidence, whereas, the 588 and 812 keV γ rays were observed only in coincidence with the 748 keV γ ray. This is evident from the coincidence spectra corresponding to the 588 and 922 keV transitions shown in Figs. 3(c) and 3(d) respectively. Similarly, the 630 keV γ -ray was found to be in coincidence with the 748-922-135 keV cascade, but not with the 971, 588, and 812 keV γ rays. A coincidence spectrum corresponding to the 630 keV γ -ray gate is also shown in

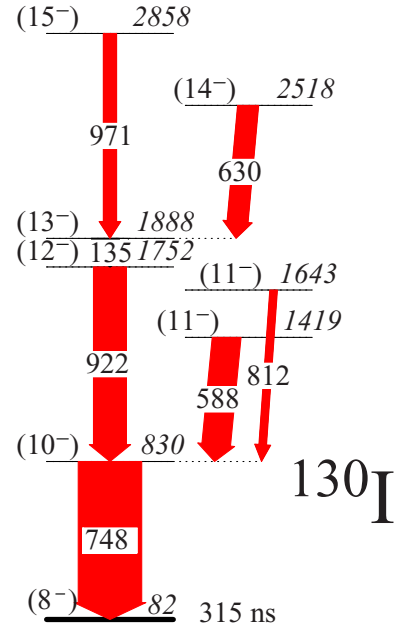


FIG. 2. Level scheme of ^{130}I above the (8^-) isomeric level, as obtained in the present work. The newly observed γ rays are displayed in red. The thickness of the γ rays represents their relative intensities.

Fig. 3(e), where the presence of the 748, 922, and 135 keV γ rays is clearly visible. Other transitions, i.e., 397, 465, and 607 keV γ rays, are also observed in the prompt spectrum and are marked in Fig. 3(a), but no coincidence could be obtained with other prompt γ rays in ^{130}I , observed in the present work. These transitions were also previously reported in Ref. [32], but the γ rays which are reported to be in coincidence with these transitions in Ref. [32], are not observed in the present work. There are a few more γ rays of energies 340, 375, 444, 557, 738, and 1091 keV, which are identified as belonging to ^{130}I and marked in the total singles spectrum [Fig. 3(a)], but could not be placed in the level scheme due to lack of coincidence information.

The isomers in ^{130}I decay via low energy γ -ray transitions ($E_\gamma < 100$ keV). The low energy cutoff for the delayed γ -ray spectra in the present setup was around 80–100 keV, thus the decay γ rays from these low lying isomers could not be

TABLE I. Energies (E_γ) and relative intensities (I_γ) of the γ rays observed in ^{130}I along with tentative spin and parity of the initial (J_i^π) and the final (J_f^π) states and the energy of the initial state (E_i).

E_γ (Err) (keV)	E_i (keV)	I_γ (Err)	$J_i^\pi \rightarrow J_f^\pi$
135.3(2)	1887.5	44(9)	(13^-) \rightarrow (12^-)
588.1(1)	1418.5	45(10)	(11^-) \rightarrow (10^-)
630.1(3)	2517.6	31(11)	(14^-) \rightarrow (13^-)
748.4(2)	830.4	100	(10^-) \rightarrow (8^-)
812.4(1)	1642.8	12(7)	(11^-) \rightarrow (10^-)
921.8(1)	1752.2	52(10)	(12^-) \rightarrow (10^-)
970.9(1)	2858.4	21(6)	(15^-) \rightarrow (13^-)

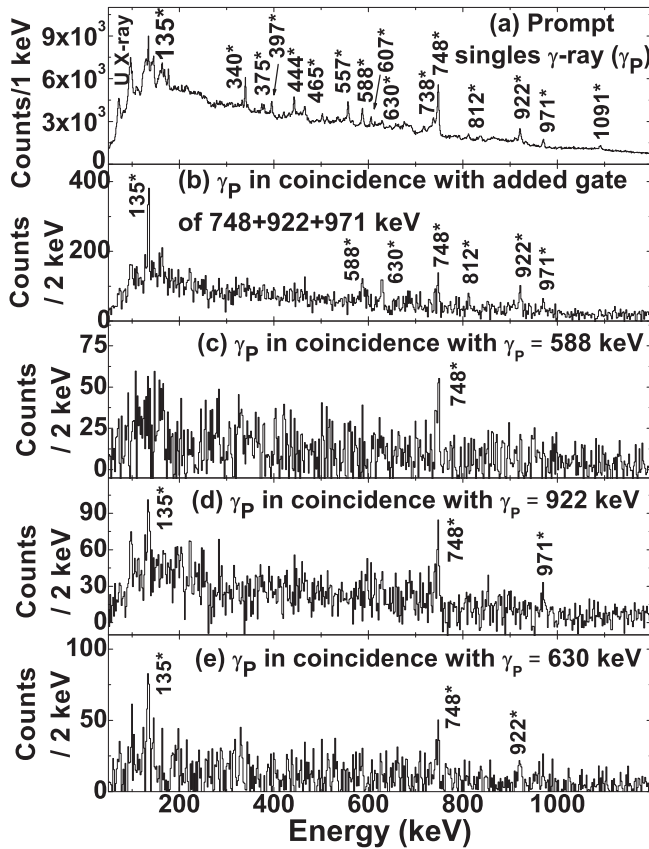


FIG. 3. (a) The prompt singles γ -ray spectrum (γ_p) of ^{130}I . (b) Prompt γ rays (γ_p) in coincidence with added gates of $\gamma_p = 748 + 922 + 971$ keV. (c) Prompt γ rays (γ_p) in coincidence with $\gamma_p = 588$ keV. (d) Prompt γ rays (γ_p) in coincidence with $\gamma_p = 922$ keV. (e) Prompt γ rays (γ_p) in coincidence with $\gamma_p = 630$ keV. The new γ transitions are marked with “*” in all the cases.

observed in the delayed spectrum obtained in the present work. Therefore, the definite placement of the observed sequence of prompt transitions above the particular isomeric state is not possible. However, following the systematics of neighboring even- A iodine isotopes, the observed prompt γ rays from the present work have been placed above the (8^-) isomer.

B. ^{131}I

Low lying states of ^{131}I were previously studied using β decay of ^{131}Te [35–37] and $(^3\text{He}, d)$ [38]. An isomeric level at $15/2^-$ with half-life 5.9 ns was reported from β -decay studies [35]. The only in-beam spectroscopic study of ^{131}I , prior to the present work, was carried out using a multi-nucleon transfer reaction [17], where three new isomers were identified at 1918 keV $19/2^-$, 2350 keV $23/2^+$, and 4308 keV $(31/2^-/33/2^-)$ of half-lives 24 μs , 42 ns, and 25 ns respectively, along with their depopulating transitions.

The proposed level scheme of ^{131}I , as obtained from the present work, is shown in Fig. 4. The details of the γ rays of ^{131}I with spin and parity of the initial (J_i^π) and the final (J_f^π) states are given in Table II. The Doppler corrected prompt

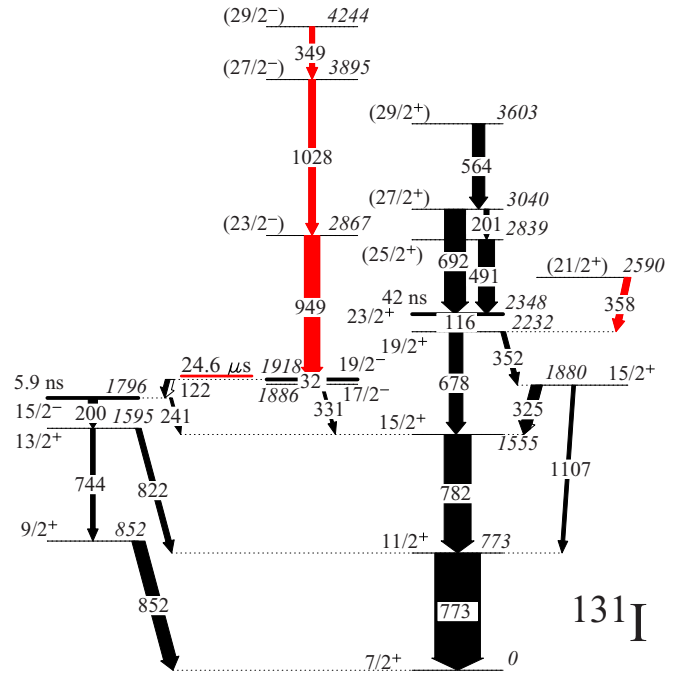


FIG. 4. Level scheme of ^{131}I as obtained in the present work. The newly observed γ rays are displayed in red. Isomeric states are indicated with a thick line and the half-life remeasured in this work is underlined by a red line. The thickness of the γ rays represents their relative intensities.

singles γ -ray spectrum (γ_p), in coincidence with ^{131}I fragments, is shown in Fig. 5(a). The newly observed γ -ray transitions from the present measurement are marked with “*” in the figure. All the other identified γ rays were previously reported in Ref. [17]. Figure 5(b) represents the added coincidence gates of prompt γ rays of 773 and 782 keV. All the γ rays which are in prompt coincidence with these two γ rays are present in this spectrum. The expanded energy range of 300–400 keV of this prompt coincidence spectrum is shown in the inset of Fig. 5(b). The presence of 325, 331, 352, and 358 keV prompt γ rays is clearly visible from the inset. The 358 keV γ ray is the new transition observed in the present work and is placed in the level scheme (Fig. 4) between the 2590 and 2232 keV levels. The other two new γ rays of 607 and 613 keV, observed in the present work, could not be placed in the level scheme, as no coincidence of these γ rays are found with other known transitions of ^{131}I . It is also evident that though the 949, 1028, and 349 keV new γ rays are observed in the prompt singles γ -ray spectrum [Fig. 5(a)], but are not present in prompt coincidence with 773 or 782 keV [Fig. 5(b)]. Prompt γ rays in coincidence with added gates of 692, 491, 201, and 564 keV γ rays, confirming the transitions placed above the $23/2^+$ (42 ns) isomeric level, are shown in Fig. 5(c). The other prompt γ rays above the $23/2^+$ level, reported in Ref. [17], of energy 765, 1055, 1202, 702, and 1266 keV, could not be observed in the present work. Figure 5(d) represents the coincidence gate of the 1028 keV transition, which shows that the 949 and 349 keV γ rays are in prompt coincidence with 1028 keV. But these γ rays are

TABLE II. Energies (E_γ) and relative intensities (I_γ) of the γ rays observed in ^{131}I along with spin and parity of the initial (J_i^π) and the final (J_f^π) states and the energy of the initial state (E_i). The top and bottom panels, separated by a line, are for the prompt and delayed transitions, respectively. The intensity scales of prompt and delayed transitions are different. The low-energy transitions which could not be detected with the present setup are adopted from Ref. [17] and are put within parentheses.

E_γ (Err) (keV)	E_i (keV)	I_γ (Err)	$J_i^\pi \rightarrow J_f^\pi$
201.1(1)	3039.8	10(1)	$(27/2^+) \rightarrow (25/2^+)$
240.7(3)	1795.5	6(2)	$15/2^- \rightarrow 15/2^+$
325.2(2)	1879.9	23(9)	$15/2^+ \rightarrow 15/2^+$
330.9(2)	1885.6	6(2)	$17/2^- \rightarrow 15/2^+$
348.6(2)	4243.7	11(3)	$(29/2^-) \rightarrow (27/2^-)$
352.2(2)	2232.2	10(1)	$19/2^+ \rightarrow 15/2^+$
358.2(3)	2590.4	14(2)	$(21/2^+) \rightarrow 19/2^+$
490.5(1)	2838.7	35(1)	$(25/2^+) \rightarrow 23/2^+$
563.6(1)	3603.4	27(2)	$(29/2^+) \rightarrow (27/2^+)$
677.5(1)	2232.2	30(3)	$19/2^+ \rightarrow 15/2^+$
691.8(1)	3039.8	46(2)	$(27/2^+) \rightarrow 23/2^+$
773.1(1)	773.1	100	$11/2^+ \rightarrow 7/2^+$
781.6(2)	1554.7	59(2)	$15/2^+ \rightarrow 11/2^+$
822.3(1)	1595.4	12(2)	$13/2^+ \rightarrow 11/2^+$
851.9(1)	851.9	28(2)	$9/2^+ \rightarrow 7/2^+$
949.1(1)	2866.7	34(1)	$(23/2^-) \rightarrow 19/2^-$
1028.4(1)	3895.1	15(2)	$(27/2^-) \rightarrow (23/2^-)$
1106.9(3)	1879.9	8(1)	$15/2^+ \rightarrow 11/2^+$
(32)	1917.6		$19/2^- \rightarrow 17/2^-$
(116)	2348.2		$23/2^+ \rightarrow 19/2^+$
122.1(1)	1917.6	34(5)	$19/2^- \rightarrow 15/2^-$
199.9(2)	1795.5	14(4)	$15/2^- \rightarrow 13/2^+$
743.8(1)	1595.6	15(2)	$13/2^+ \rightarrow 9/2^+$

not in prompt coincidence with any other transitions placed in ^{131}I .

Figure 6(a) shows the delayed singles γ -ray (γ_D) spectrum obtained with EXOGAM detectors for $t_{\text{Decay}} < 75 \mu\text{s}$, following the procedure described in Ref. [28]. All the delayed γ rays below the 1918 keV ($19/2^-$) isomeric level are seen in this spectrum. The decay curve corresponding to the 122 + 331 keV delayed γ rays is shown in the inset of Fig. 6(a) within the same time window. An exponential fit to the time decay corresponding to the added gates of 122 and 331 keV γ rays yield a half-life of $T_{1/2} = 24.6(52) \mu\text{s}$ for the 1918 keV ($19/2^-$) level from the present measurements. The measured half-life of the 1918 keV ($19/2^-$) level corroborates the reported value of 24(1) μs [17]. The delayed γ -ray (γ_D) spectrum for $t_{\text{Decay}} < 75 \mu\text{s}$ in coincidence with the newly observed prompt transition of 949 keV is shown in Fig. 6(b). The delayed γ rays deexciting the $19/2^-$ isomeric level are seen in this spectrum. This confirms the placement of the 949 keV prompt γ -ray above the 1918 keV ($19/2^-$) isomeric level. Figure 6(c) shows the prompt γ -ray (γ_P) spectrum corresponding to the gate on the delayed γ -ray 122 keV. The presence of the 949 keV γ -ray in this coincidence spectrum and the mutual prompt coincidence among the 949, 1028,

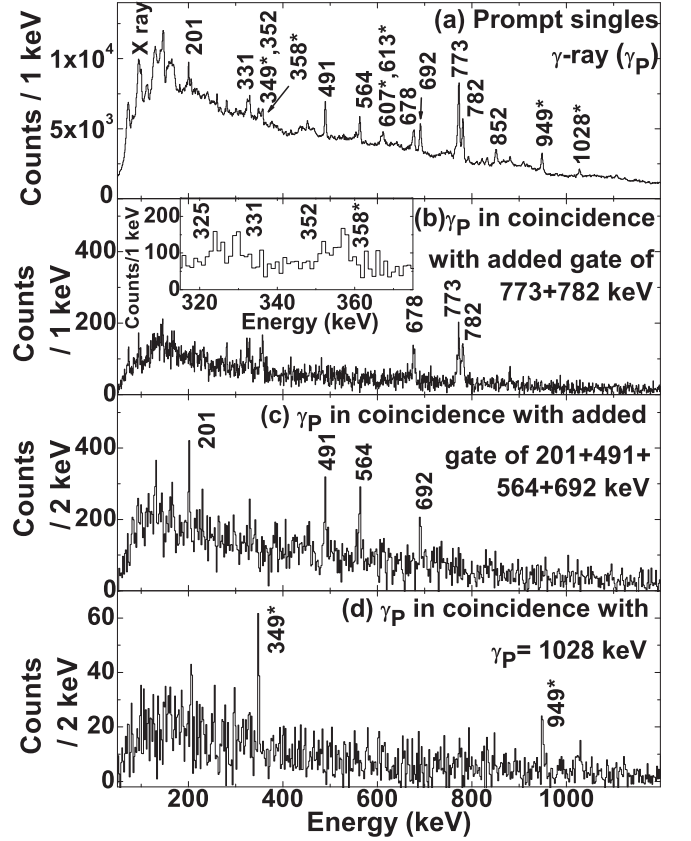


FIG. 5. (a) The prompt singles γ -ray spectrum of ^{131}I . (b) Prompt γ rays (γ_P) in coincidence with added gates of $\gamma_P = 773 + 782$ keV. The inset shows the expanded energy range of 300–400 keV. (c) Prompt γ rays (γ_P) in coincidence with added gates of $\gamma_P = 201 + 491 + 564 + 692$ keV. (d) Prompt γ rays (γ_P) in coincidence with $\gamma_P = 1028$ keV. The new γ transitions are marked with “*”.

and 349 keV γ rays [as shown in Fig. 5(d)] establishes the placement of prompt γ -ray cascade of 949–1028–349 keV above the 1918 keV ($19/2^-$) isomeric level. The γ rays of this sequence are placed according to their intensities.

C. ^{132}I

Excited states of ^{132}I were studied earlier using β -decay of ^{132}Te , produced from the α -induced fission [39]. In this β -decay study, only the low spin states were populated. The lifetime and magnetic moment measurements of low spin states have been reported in various investigations [40–42]. The presence of an isomeric state (8^- , $T_{1/2} = 83.6 \pm 1.7$ min) at 120 keV excitation was also reported in Ref. [39,41]; it was populated in an α -induced fission reaction. No information of the high-spin states above this long lived (8^-) isomer was available.

The proposed level scheme of ^{132}I , as obtained from the present work, is shown in Fig. 7. All the γ rays, marked in the level scheme with red color, are observed for the first time. The γ rays are placed in the level scheme according to their prompt-prompt and prompt-delayed coincidence relations and relative intensities. The proposed level scheme

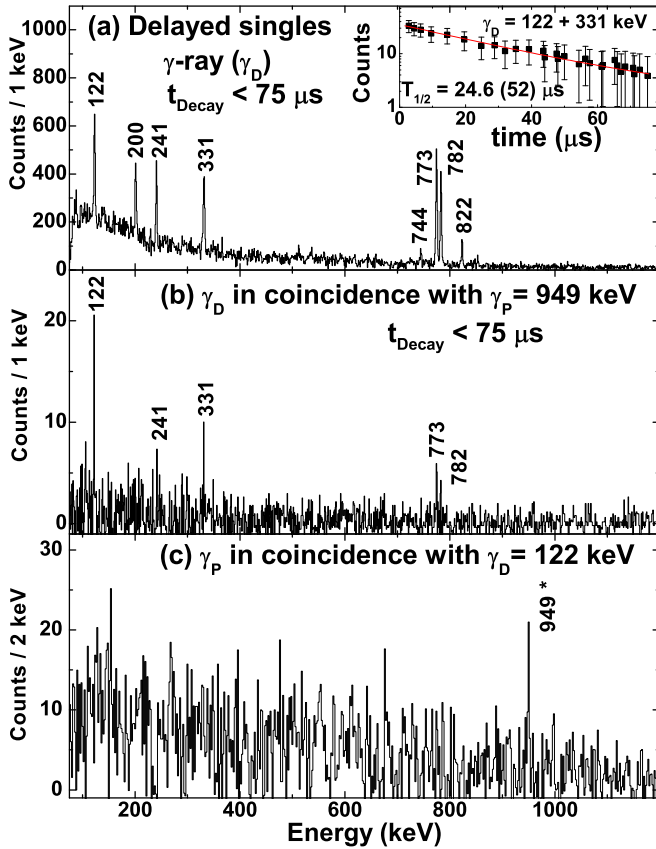


FIG. 6. (a) The delayed singles γ -ray (γ_D) spectrum of ^{132}I for $t_{\text{Decay}} < 75 \mu\text{s}$. The inset shows the decay curve of $\gamma_D = 122 + 331$ keV delayed transitions with exponential fit. (b) Delayed γ rays (γ_D) for $t_{\text{Decay}} < 75 \mu\text{s}$ in coincidence with $\gamma_P = 949$ keV. (c) Prompt γ rays (γ_P) in coincidence with $\gamma_D = 122$ keV. The new γ transitions are marked with “*”.

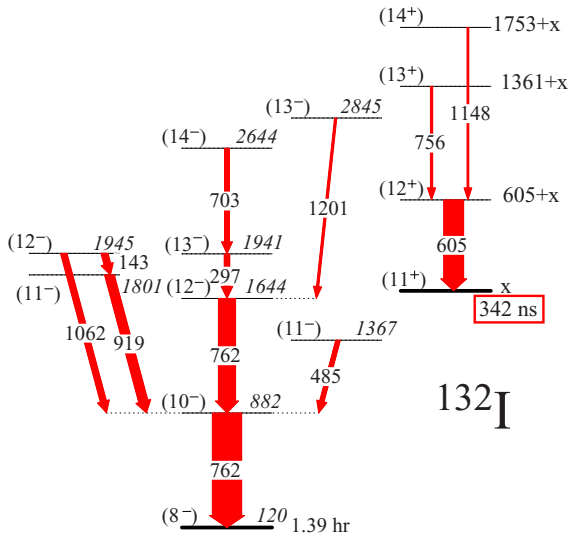


FIG. 7. Level scheme of ^{132}I above the (8^-) isomeric level, as obtained in the present work. The newly observed γ rays are displayed in red. The isomeric state is indicated with a thick line and the newly measured half-life has been marked with a red box. The thickness of the γ rays represents their relative intensities with respect to the 762 keV doublet.

TABLE III. Energies (E_γ) and relative intensities (I_γ) of the γ rays observed in ^{132}I along with probable spin and parity of the initial (J_i^π) and the final (J_f^π) states and the energy of the initial state (E_i). The total intensity of the 762 keV doublet (d) is normalized to 100.

E_γ (Err) (keV)	E_i (keV)	I_γ (Err)	$J_i^\pi \rightarrow J_f^\pi$
143.3(2)	1944.6	12(2)	$(12^-) \rightarrow (11^-)$
296.9(1)	1941.3	12(1)	$(13^-) \rightarrow (12^-)$
484.6(1)	1366.8	10(1)	$(11^-) \rightarrow (10^-)$
605.4(1)	605 + x	44(1)	$(12^+) \rightarrow (11^+)$
703.0(1)	2644.3	11(2)	$(14^-) \rightarrow (13^-)$
755.7(2)	1361 + x	2(1)	$(13^+) \rightarrow (12^+)$
762.2(4)	1644.4	100 ^d	$(12^-) \rightarrow (10^-)$
762.2(4)	882.2		$(10^-) \rightarrow (8^-)$
919.2(3)	1801.4	21(2)	$(11^-) \rightarrow (10^-)$
1062.4(2)	1944.6	14(1)	$(12^-) \rightarrow (10^-)$
1147.8(2)	1753 + x	4(1)	$(14^+) \rightarrow (12^+)$
1200.9(2)	2845.3	5(2)	$(13^-) \rightarrow (12^-)$

(Fig. 7) from the present work is placed on top of the (8^-) isomeric state. No coincidences were observed between the previously known transitions and the newly observed γ rays from the present work. Due to the very long lifetime of the (8^-) isomer, prompt-delayed coincidence measurement across this isomer was not possible in the present experiment. The details of the γ rays of ^{132}I with tentative spin and parity assignments of the initial (J_i^π) and final (J_f^π) states are tabulated in Table III. A Doppler corrected prompt singles γ -ray (γ_P) spectrum, obtained with AGATA, in coincidence with ^{132}I fragments, isotopically (A, Z) identified at the focal plane of the VAMOS++ spectrometer, is shown in Fig. 8(a). In this spectrum, the new γ rays observed from the present work are marked with “*”. A prompt γ - γ coincidence spectrum corresponding to the gate of the 762 keV γ -ray is shown in Fig. 8(b). The presence of a 762 keV transition in the 762 keV gate establishes 762 keV as a doublet transition. Other than the 762 keV transition, the 143, 297, 485, 703, 919, 1062, and 1201 keV transitions are also found to be in coincidence with the 762 keV γ ray. The 762 keV doublet and the other transitions observed in the 762 keV gate are placed in the level scheme of ^{132}I (Fig. 7) according to their relative intensities. Among the transitions observed in the 762 keV gate, those at 297, 485, 919, 1062, and 1201 keV are not found to be in coincidence with each other. The 143 keV transition is found to be in coincidence with 762 and 919 keV transitions, but not with 1062 keV. Thus, the 919-143 keV cascade is placed in parallel with 1062 keV from coincidence relationship, intensities, and energy sum. The observed intensity of the 762 keV γ ray in the coincidence spectra of the 297, 919, 1062, and 1201 keV gates is compared to understand the relative placements of these transitions in the level scheme. The intensity of the 762 keV γ ray is found to be more in the coincidence spectra of the 297 and 1201 keV gates than in the coincidence spectra of the 1062 and 919 keV gates, after appropriate intensity normalization of the gating transitions. Thus, it is clear that the 1062 and 919 keV γ rays are in coincidence with one of

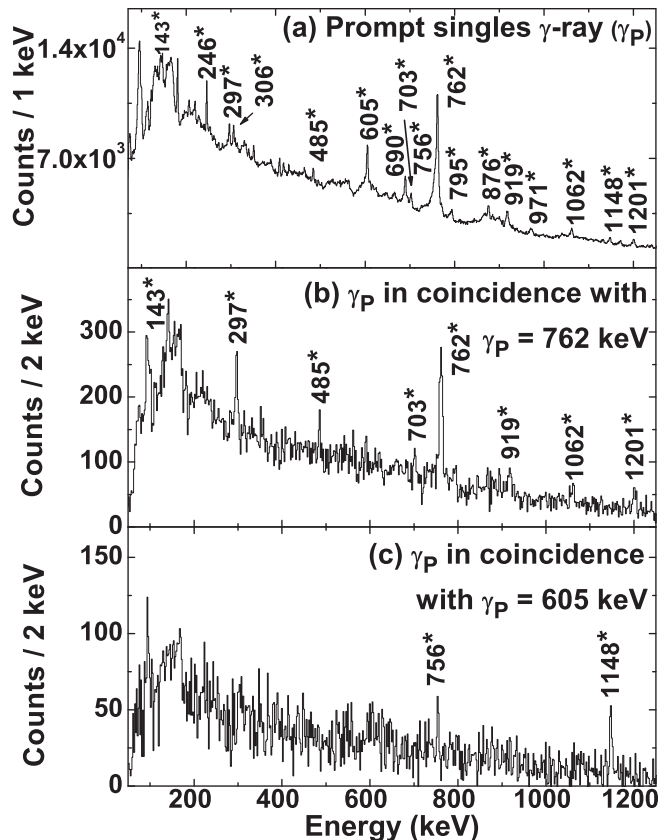


FIG. 8. (a) The prompt singles γ -ray spectrum of ^{132}I . (b) Prompt γ rays (γ_P) in coincidence with $\gamma_P = 762$ keV. (c) Prompt γ rays (γ_P) in coincidence with $\gamma_P = 605$ keV. The new γ transitions are marked with “*”.

the transitions of the 762 keV doublet, whereas those at 297 and 1201 keV are in coincidence with both the transitions of the 762 keV doublet. Also the 605, 756, and 1148 keV γ rays are seen in the prompt singles (γ_P) spectrum [Fig. 8(a)], but are not in coincidence with the 762 keV γ ray [Fig. 8(b)]. The 756 and 1148 keV transitions are found to be present in the coincidence spectrum corresponding to the 605 keV gate, as shown in Fig. 8(c). On the other hand, no coincidence could be found between the 756 and 1148 keV transitions and hence these are placed in parallel with each other. The set of transitions of energy 605, 756, and 1148 keV do not have any prompt coincidence with any other γ rays of the prompt sequence. The γ rays of energies 246, 306, 690, 795 and 876 keV, observed in the prompt singles γ -ray spectrum [Fig. 8(a)], could not be placed in the level scheme of ^{132}I , as these are not observed to be in coincidence with other γ rays in ^{132}I .

The delayed singles γ -ray (γ_D) spectrum obtained with the EXOGAM detectors for $t_{\text{Decay}} < 3$ μs is shown in Fig. 9(a). Only the 762 keV transition was found to be in this delayed coincidence. The inset of Fig. 9(a) shows the fitting of the decay curve of the 762 keV transition, from which the half-life is obtained as $T_{1/2} = 342(12)$ ns. The delayed γ rays (γ_D) within the same time window, in coincidence with the prompt

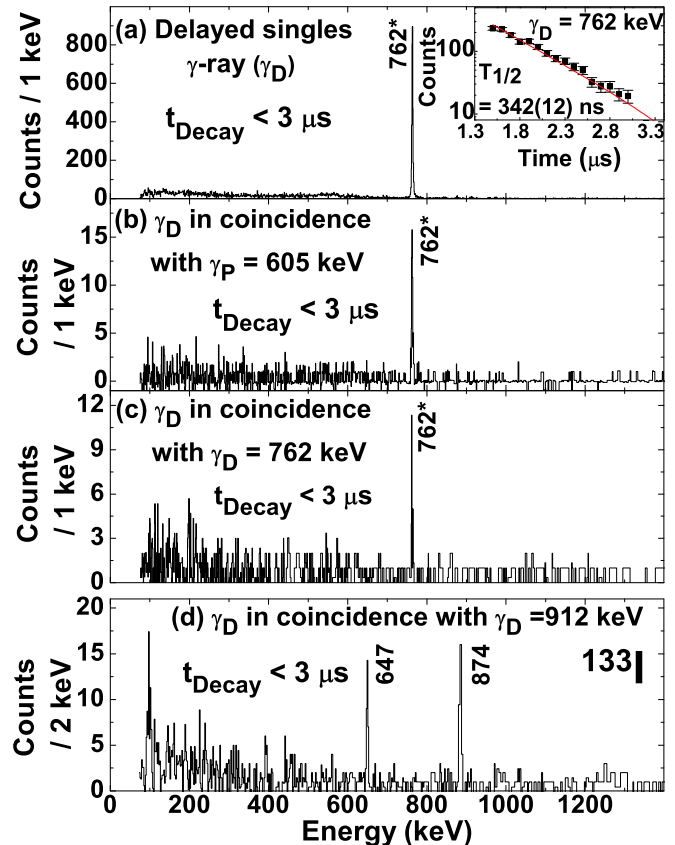


FIG. 9. (a) The delayed singles γ -ray (γ_D) spectrum of ^{132}I for $t_{\text{Decay}} < 3$ μs . The inset shows the decay pattern of the delayed γ ray of 762 keV with exponential fitting. (b) Delayed γ rays (γ_D) for $t_{\text{Decay}} < 3$ μs in coincidence with $\gamma_P = 605$ keV. (c) Delayed γ rays (γ_D) for $t_{\text{Decay}} < 3$ μs in coincidence with $\gamma_D = 762$ keV. (d) Delayed γ rays (γ_D) for $t_{\text{Decay}} < 3$ μs in coincidence with $\gamma_D = 912$ keV of ^{133}I . The new γ transitions are marked with “*”.

transition $\gamma_P = 605$ keV, are shown in Fig. 9(b). Thus, the 605, 756, and 1148 keV transitions, which are in prompt coincidence with each other, must be placed as prompt transitions above this isomer. Figure 9(c) shows the delayed γ rays observed in coincidence with the delayed transition $\gamma_D = 762$ keV. It is evident from this spectrum that the transitions of the 762 keV doublet form a cascade below the isomer. To verify the correctness of the γ_D - γ_D coincidence procedure, the gate was put on the delayed γ ray of 912 keV of ^{133}I with a known cascade below the 478 ns, $23/2^+$ isomer at 2492 keV (see the text in the next section also). From Fig. 9(d), the presence of the known γ rays of this cascade is evident. The 59 keV γ -ray decaying from the $23/2^+$ isomer in ^{133}I could not be observed due to the threshold at low energy (80–100 keV). Since, in ^{132}I , the 762 keV doublet and the 297 and 703 keV transitions are in prompt coincidence [see Fig. 9(b)], neither of the corresponding depopulated levels are isomeric. Therefore, the isomer is likely to be depopulated by a low energy unobserved transition. Thus the excitation energy of the 342 ns isomer, found in ^{132}I , is marked as “x” in the level scheme (Fig. 7). The spin-parity of this state is tentatively

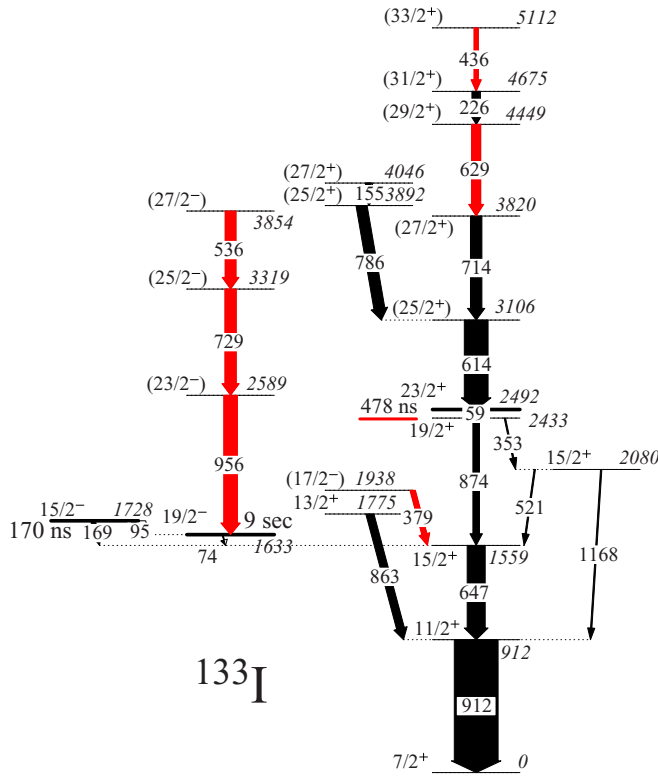


FIG. 10. Level scheme of ^{133}I as obtained in the present work. The newly observed γ rays are displayed in red. The isomeric state is indicated with a thick line and the half-life remeasured in this work has been underlined by a red line. The thickness of the γ rays represents their relative intensities.

assigned as (11^+) by comparing with the similar isomeric state in Sb isotopes (see Sec. IV B).

D. ^{133}I

Spectroscopic information of the low spin states of ^{133}I was first extracted from β -decay measurements [43,44]. High-spin spectroscopy of ^{133}I was carried out via multi-nucleon transfer reaction [17]. In Ref. [17], three isomers of half-lives 170 ns, 9 s, and 469 ns were reported at 1728 keV $15/2^-$, 1634 keV $19/2^-$, and 2493 keV $23/2^+$ respectively.

The proposed level scheme of ^{133}I , from the present work, is shown in Fig. 10. The details of the γ rays of ^{133}I with the spin-parity assignments of the initial (J_i^π) and the final (J_f^π) states are tabulated in Table IV. The Doppler corrected prompt singles γ -ray (γ_p) spectrum, obtained with AGATA, in coincidence with ^{133}I fragments, after (A, Z) selection at the focal plane of the VAMOS++ spectrometer, is shown in Fig. 11(a). The new γ rays observed in the present work are marked with “*”. The higher energy part of the prompt singles γ -ray (γ_p) spectrum is shown in an expanded scale in the inset of Fig. 11(a). The presence of the 1168 keV γ ray, placed in the level scheme from previous measurements [17], is clear from this spectrum. Four of the new γ rays of 311, 1078, 1083, and 1179 keV, observed from the present work [marked with “*” in Fig. 11(a)], could not be placed in the level scheme due

TABLE IV. Energies (E_γ) and relative intensities (I_γ) of the γ rays observed in ^{133}I along with probable spin and parity of the initial (J_i^π) and the final (J_f^π) states and the energy of the initial state (E_i). The top and bottom panels, separated by a line, are for the prompt and delayed transitions, respectively. The low-energy transitions which could not be detected with the present setup are adopted from Ref. [17] and are put within parentheses.

E_γ (Err) (keV)	E_i (keV)	I_γ (Err)	$J_i^\pi \rightarrow J_f^\pi$
154.6(1)	4046.3	12(2)	$(27/2^+) \rightarrow (25/2^+)$
226.2(1)	4675.3	18(1)	$(31/2^+) \rightarrow (29/2^+)$
352.8(2)	2433.2	3(1)	$19/2^+ \rightarrow 15/2^+$
378.5(1)	1937.6	12(1)	$(17/2^-) \rightarrow 15/2^+$
436.2(2)	5111.5	10(1)	$(33/2^+) \rightarrow (31/2^+)$
521.3(1)	2080.5	3(1)	$15/2^+ \rightarrow 15/2^+$
535.6(2)	3854.2	25(3)	$(27/2^-) \rightarrow (25/2^-)$
614.0(1)	3105.9	54(1)	$(25/2^+) \rightarrow 23/2^+$
629.2(1)	4449.1	21(1)	$(29/2^+) \rightarrow (27/2^+)$
647.0(1)	1559.1	41(2)	$15/2^+ \rightarrow 11/2^+$
714.0(1)	3819.9	26(1)	$(27/2^+) \rightarrow (25/2^+)$
729.2(1)	3318.6	26(2)	$(25/2^-) \rightarrow (23/2^-)$
785.8(1)	3891.7	25(1)	$(25/2^+) \rightarrow (25/2^+)$
862.7(1)	1774.8	18(2)	$13/2^+ \rightarrow 11/2^+$
874.1(1)	2433.2	15(1)	$19/2^+ \rightarrow 15/2^+$
912.1(1)	912.1	100	$11/2^+ \rightarrow 7/2^+$
956.3(1)	2589.4	31(2)	$(23/2^-) \rightarrow 19/2^-$
1168.4(1)	2080.5	3(1)	$15/2^+ \rightarrow 11/2^+$
(59)	2491.9		$23/2^+ \rightarrow 19/2^+$
(74)	1633.1		$19/2^- \rightarrow 15/2^+$
(95)	1728.1		$15/2^- \rightarrow 19/2^-$
(169)	1728.1		$15/2^- \rightarrow 15/2^+$

to the low statistics in the corresponding coincidence spectra. However, their assignment to ^{133}I is confirmed as the prompt singles γ -ray (γ_p) spectrum is obtained with (A, Z) gating condition. The prompt γ - γ coincidence spectra corresponding to the added gates of 912, 647, and 874 keV γ rays below the isomeric levels is shown in Fig. 11(b). The 379 keV γ ray is newly observed from the present work and, on the basis of the coincidence relation, it has been placed above the 1559 keV level. In the present work, the high-spin states of ^{133}I above the $23/2^+$ isomer have been extended with addition of two new transitions of 629 and 436 keV. A prompt γ - γ coincidence spectrum corresponding to the sum gates of 614, 714, and 629 keV, decaying to the $23/2^+$ isomeric level, is shown in Fig. 11(c). The new γ rays of energy 629 and 436 keV, placed in the proposed level scheme above the $23/2^+$ isomer, are clearly seen in this coincidence spectrum. The placement of the previously reported 226 keV transition has also been changed on the basis of measured relative intensities in the present work. The other new γ rays, i.e., 956, 729, and 536 keV, observed in the prompt spectrum [Fig. 11(a)], are found to be in coincidence with each other, but not with any other known prompt γ -ray transitions of ^{133}I . This is evident from the added coincidence gates of 956, 729, and 536 keV γ rays, shown in Fig. 11(d). Also, no prompt-delayed correlation is found for these γ rays. However, the assignment

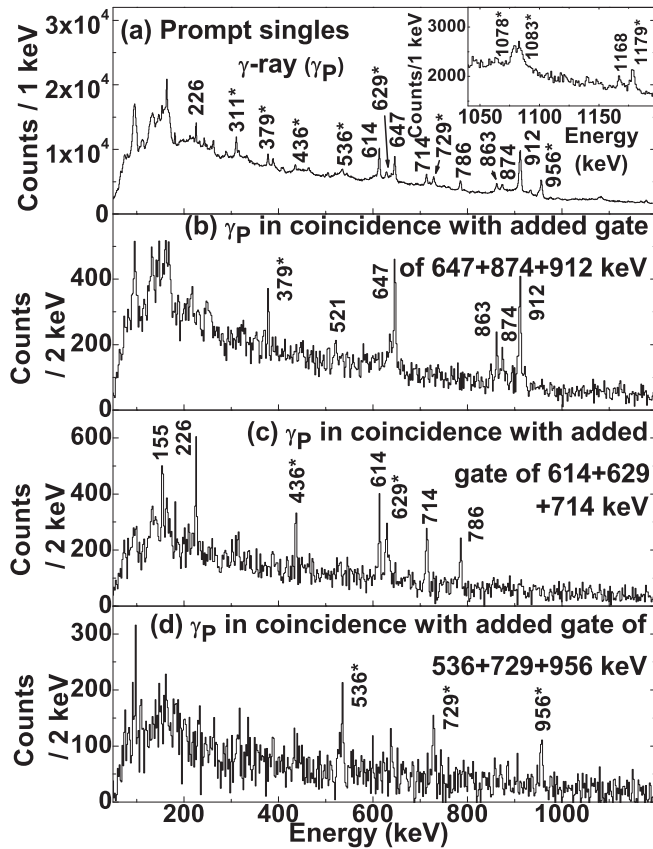


FIG. 11. (a) The prompt singles γ -ray spectrum of ^{133}I . The higher energy part of this spectrum is shown in an expanded scale in the inset. (b) Prompt γ rays (γ_P) in coincidence with the added gate of $\gamma_P = 647 + 874 + 912$ keV. (c) Prompt γ rays (γ_P) in coincidence with added gate of $\gamma_P = 614 + 629 + 714$ keV. (d) Prompt γ rays (γ_P) in coincidence with added gate of $\gamma_P = 536 + 729 + 956$ keV. The new γ transitions are marked with “*” in all the cases.

of these γ rays to ^{133}I could be confirmed from their presence in the prompt γ -ray spectrum [Fig. 11(a)], obtained after isotopic (A, Z) selection of ^{133}I fragments. It may be noted that a similar set of prompt γ rays have been observed in the neighboring odd- A ^{131}I , above the $19/2^-$ isomer ($24.6 \mu\text{s}$). Thus, it is possible that the new cascade of prompt transitions of 956 - 729 - 536 keV observed in ^{133}I may also decay to the $19/2^-$ (9 s) isomeric state. As the upper limit ($200 \mu\text{s}$) of the delayed time window for the present setup is much lower than the half-life of the $19/2^-$ (9 s) isomeric state in ^{133}I , the prompt-delayed correlation across the isomer cannot be obtained. Therefore, the cascade of prompt transitions of 956 - 729 - 536 keV is placed above the $19/2^-$ (9 s) isomeric state at 1633 keV in ^{133}I .

Figure 12(a) shows the delayed singles γ -ray (γ_D) spectrum for $t_{\text{Decay}} < 3 \mu\text{s}$. All the known delayed γ rays of ^{133}I , i.e., 912 , 647 , 874 , 1168 , and 353 keV, are observed in this time gated delayed spectrum. The other known delayed low energy γ rays of 59 , 74 , 95 , and 169 keV could not be observed in this delayed spectrum, either due to their weak intensities or due to the low energy threshold of the present setup to detect delayed γ rays. The time decay curve for

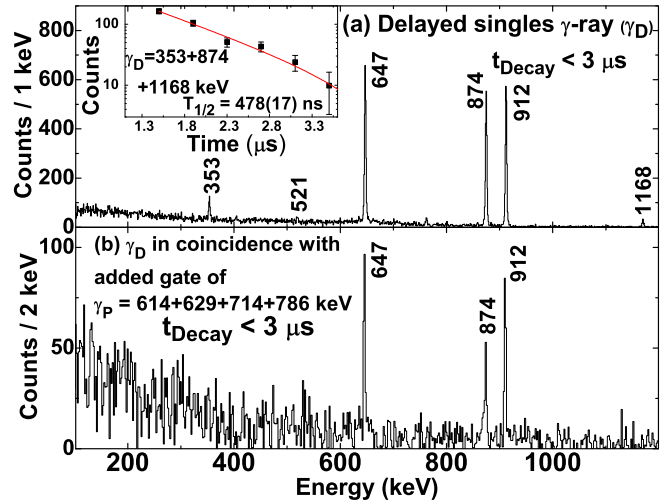


FIG. 12. (a) Delayed γ -ray (γ_D) spectrum of ^{133}I for $t_{\text{Decay}} < 3 \mu\text{s}$. The inset of the figure shows the decay pattern of delayed γ rays $\gamma_D = 353 + 874 + 1168$ keV with exponential fitting. (b) Delayed γ rays (γ_D) in coincidence with the added prompt gate of $\gamma_P = 614 + 629 + 714 + 786$ keV. $t_{\text{Decay}} < 3 \mu\text{s}$.

the $874 + 353 + 1168$ keV transitions, decaying out from the $23/2^+$ isomer, is shown in the inset of Fig. 12(a). An exponential decay fit of this curve yields a value of $T_{1/2} = 478(17)$ ns, which matches well with the reported [17] value of $469(15)$ ns. Figure 12(b) shows the delayed γ rays observed in coincidence with the prompt transitions of 614 , 714 , 629 , and 785 keV above the $23/2^+$ isomer. The known delayed transitions of 912 , 647 , and 874 keV below the isomer are clearly seen in this spectrum. The other γ rays of 353 , 521 , and 1168 keV could not be seen in this spectrum due to their weak intensities.

E. ^{134}I

Low lying excited states of ^{134}I were previously studied from β decay of ^{134}Te [45,46]. A high-spin isomer (8^-) of $T_{1/2} \approx 3.8 \pm 0.2$ m (adopted in NNDC as 3.52 ± 0.04 m [47]) at an excitation energy of 316 keV was also identified in Ref. [48]. High-spin states above the (8^-) isomer in ^{134}I were recently investigated using prompt spectroscopy of fission fragments [18] where five excited states were identified. The assignment of γ rays to ^{134}I was done in Ref. [18] on the basis of intensity distribution of its complementary fragments.

The level scheme of ^{134}I , as obtained from the present measurements, is shown in Fig. 13. In the present work, the level scheme above the reported (8^-) isomer of ^{134}I , as reported by Liu et al. [18], is extended with the placement of one new γ -ray transition ($17^+ \rightarrow 14^-$) above the 3689 keV level (see discussions in Sec. IV B). The assignment of the earlier known γ rays and the newly observed γ ray from the present work were confirmed after unambiguous isotopic (A, Z) identification of ^{134}I . The details of the γ rays of ^{134}I with probable spin and parity of the initial (J_i^π) and the final (J_f^π) states are tabulated in Table V. A Doppler corrected prompt singles γ -ray spectrum (γ_P), obtained with AGATA,

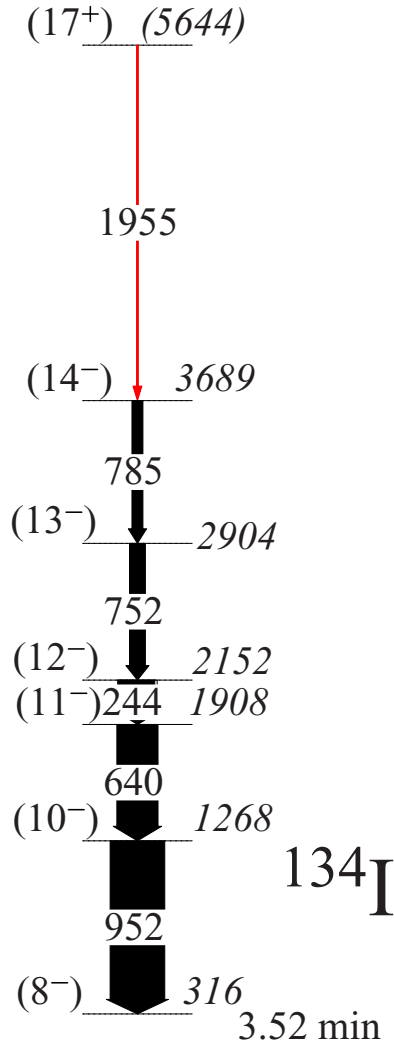


FIG. 13. Level scheme of ^{134}I as obtained in the present work. The newly observed γ rays are displayed in red. The thickness of the γ rays represents their relative intensity.

in coincidence with ^{134}I fragments, is shown in Fig. 14(a). The previously known γ -ray transitions of energy 244, 640, 752, 785, and 952 keV are marked along with one new γ ray of energy 1955 keV (marked with “*”), observed from the present

TABLE V. Energies (E_γ) and relative intensities (I_γ) of the γ rays observed in ^{134}I along with probable spin and parity of the initial (J_i^π) and the final (J_f^π) states and the energy of the initial state (E_i).

E_γ (Err) (keV)	E_i (keV)	I_γ (Err)	$J_i^\pi \rightarrow J_f^\pi$
243.5(1)	2150.9	68(1)	(12 ⁻) \rightarrow (11 ⁻)
639.6(1)	1907.4	75(1)	(11 ⁻) \rightarrow (10 ⁻)
752.0(1)	2902.9	29(2)	(13 ⁻) \rightarrow (12 ⁻)
785.2(1)	3688.1	20(1)	(14 ⁻) \rightarrow (13 ⁻)
951.8(1)	1267.8	100	(10 ⁻) \rightarrow (8 ⁻)
1955.1(1)	5643.2	3(1)	(17 ⁺) \rightarrow (14 ⁻)

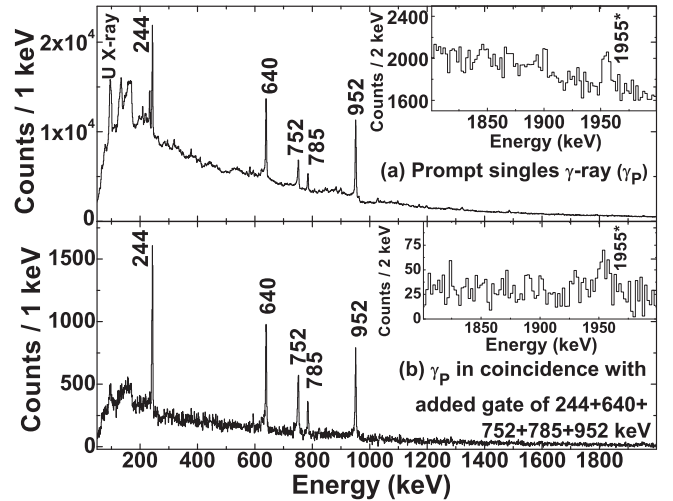


FIG. 14. (a) The prompt singles γ -ray spectrum of ^{134}I . (b) Prompt γ rays (γ_p) in coincidence with added gate of $\gamma_p = 244 + 640 + 752 + 785 + 952$ keV. The higher energy parts of the spectra are shown in insets. The new γ transitions are marked with “*” in all the cases.

work. The prompt γ - γ coincidence spectrum corresponding to the added prompt gates on 952, 640, 244, 752, and 785 keV transitions is shown in Fig. 14(b). All the previously assigned transitions along with 1955 keV (marked with “*”) are seen in this figure. The presence of the 1955 keV γ ray in this added spectrum is clear from the inset of Fig. 14(b), where the higher energy part of the coincidence spectrum is shown in an expanded energy scale. The new transition is tentatively placed in the level scheme of ^{134}I , based on the coincidence spectra shown in the inset of Fig. 14(b), above the 3689 keV level. No delayed γ rays (γ_d) could be observed in ^{134}I in the present work.

IV. DISCUSSION

A. Systematics

The systematics of the energy difference between the low-lying $\Delta I = 2$ states is plotted for the isotopes of Sn ($Z = 50$), Sb ($Z = 51$), Te ($Z = 52$), and I ($Z = 53$) as a function of neutron number in Fig. 15(a) for even N and in Fig. 15(b) for odd N . One can observe the change in the energy differences as one, two, and three protons are added to the corresponding Tin core (Sn_N). In Sb, the energy differences $E(11/2^+) - E(7/2^+)$ and $E(10^-) - E(8^-)$ follow closely the corresponding $E(2^+) - E(0^+)$ and $E(15/2^-) - E(11/2^-)$ in Sn, respectively. This reflects the fact that the energy difference results from the neutron excitation, i.e., 2^+ , in both Sn and Sb, since the proton is either absent in Sn or singly present in Sb. It can be also seen that in I the energy differences $E(11/2^+) - E(7/2^+)$ and $E(10^-) - E(8^-)$ follow the corresponding $E(2^+) - E(0^+)$ and $E(15/2^-) - E(11/2^-)$ in Te, respectively. The significant drop in the energy difference in Te and I, relative to that in Sn and Sb, results from the strong mixing between the proton and neutron excitations due to the neutron-proton interaction. The decrease of the energy

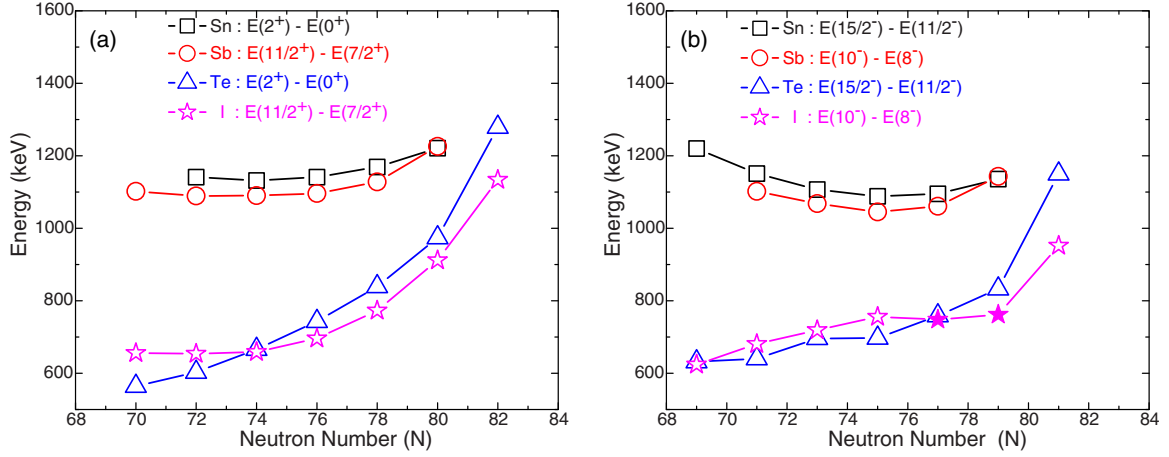


FIG. 15. Systematics of experimental energy differences for the lowest states with $\Delta I = 2$ for (a) even- N isotopes of Sn [$E(2^+) - E(0^+)$], Sb [$E(11/2^+) - E(7/2^+)$], Te [$E(2^+) - E(0^+)$], and I [$E(11/2^+) - E(7/2^+)$], and. (b) odd- N isotopes of Sn [$E(15/2^-) - E(11/2^-)$], Sb [$E(10^-) - E(8^-)$], Te [$E(15/2^-) - E(11/2^-)$], and I [$E(10^-) - E(8^-)$]. The new states observed in the present measurements are shown by filled symbols.

differences in Te and I, towards the neutron mid-shell, can be seen from the figure. The systematic energy drop, i.e., $(Z, Z + 1), (Z + 2, Z + 3), \dots$ with $Z = 50$, is related to the increase of the collectivity. A similar energy drop and an energy inheritance, for odd Z from even- Z isotones, could be also observed for other isotopes from the known data (not shown here) while more protons are added, towards the proton mid-shell.

B. Shell model calculations

To understand the basic configurations and contribution of various single-particle orbitals to the excited states of the iodine isotopes in the mass region $A = 130$ – 134 , observed in the present work, large-scale shell model calculations were performed using the code NUSHELLX [49]. The calculations were carried out using the model space involving $1g_{7/2}, 2d_{5/2}, 2d_{3/2}, 3s_{1/2}, 1h_{11/2}$ single-particle orbitals, for both protons and neutrons. The calculations used the SN100PN interaction [50]. The results of the shell model calculations are compared with the experimental levels, obtained in the present work, for even- A and odd- A iodine isotopes in Figs. 16(a)–16(c) and 16(d)–16(e) respectively. An overall good agreement is observed between the experimental and calculated levels for all the iodine isotopes.

In the present shell model calculation of the even mass isotopes ^{130}I ($N = 77$) and ^{132}I ($N = 79$), the 8^- level is predicted as the ground state, instead for the experimentally known ground states of 5^+ and 4^+ , respectively. But, the energy differences between the calculated and experimental ground states are found to be within 120 keV for both the nuclei. In the case of ^{134}I ($N = 81$), the measured ground state is reproduced in the shell model calculation as 4^+ .

The higher-spin negative parity states above the (8^-) state in $^{130,132}\text{I}$, newly observed in the present work, could be reproduced well in the shell model calculations, as can be seen from Figs. 16(a) and 16(b), respectively. The spin assignments to the negative parity levels above the (8^-) isomeric state in

both $^{130,132}\text{I}$ are based on the comparison with the present shell model calculation and the systematics of the even mass iodine isotopes. The relative excitation energies and the sequence $8^- - 10^- - 11^- - 12^-$ with respect to the (8^-) state in $^{130,132}\text{I}$ follow a smooth pattern and are very similar to the corresponding states in ^{128}I ($N = 75$) and ^{134}I ($N = 81$). Thus the excited states at 830, 1419, and 1752 keV in ^{130}I and the states at 882, 1367, and 1644 keV in ^{132}I are assigned as (10^-) , (11^-) , and (12^-) respectively. This relative energy spacing increases for higher mass number towards $N = 82$. The yrast sequence $12^- - 10^- - 8^-$ in ^{130}I and ^{132}I also closely follows the analogous sequence of $15/2^+ - 11/2^+ - 7/2^+$ in odd- A neighbors ^{129}I and ^{131}I , respectively.

The new 342 ns isomeric state in ^{132}I , reported in the present work, is tentatively assigned as (11^+) , following the systematics of similar isomers observed in even- A Sb isotopes [31]. The three new excited states observed above the (11^+) isomer in ^{132}I are assigned as (12^+) , (13^+) , and (14^+) , respectively, following the similar pattern of spin sequence above the (11^+) , 600 ns isomer, in ^{130}Sb . The excitation energy of the (11^+) isomer in ^{132}I could not be determined experimentally. The shell model calculation predicts the $\pi g_{7/2}^3 \nu d_{3/2}^{-1} \nu h_{11/2}^{-2}$ configuration as the main component of those positive parity states with an admixture of $\pi g_{7/2}^3 \nu s_{1/2}^{-1} \nu h_{11/2}^{-2}$ configuration. The excitation energy differences of the positive parity states above the (11^+) isomer are not well reproduced by the shell model calculations [Fig. 16(b)].

In ^{134}I , the yrast states, i.e., $(8^- - 14^-)$ were understood as built from the $\pi g_{7/2}^3 \nu h_{11/2}^{-1}$ and $\pi g_{7/2}^2 \pi d_{5/2} \nu h_{11/2}^{-1}$ configurations [18,51]. In this work, the newly observed state at 5644 keV decaying by the emission of the 1955 keV transition is proposed as (17^+) , resulting from the $\pi g_{7/2}^2 \pi h_{11/2}^1 \nu h_{11/2}^{-1}$ configuration, based on the following considerations. In the neighboring nucleus ^{135}I , having the closed $N = 82$ shell, the low-lying positive parity states $(7/2^+, 11/2^+, 15/2^+, 17/2^+)$ are mainly from the $\pi g_{7/2}^3$ and $\pi g_{7/2}^2 \pi d_{5/2}^1$ configurations [19,52]. The higher-lying yrast states, around 3.7 MeV $(19/2^-, 21/2^-, 23/2^-)$ have negative parity and are

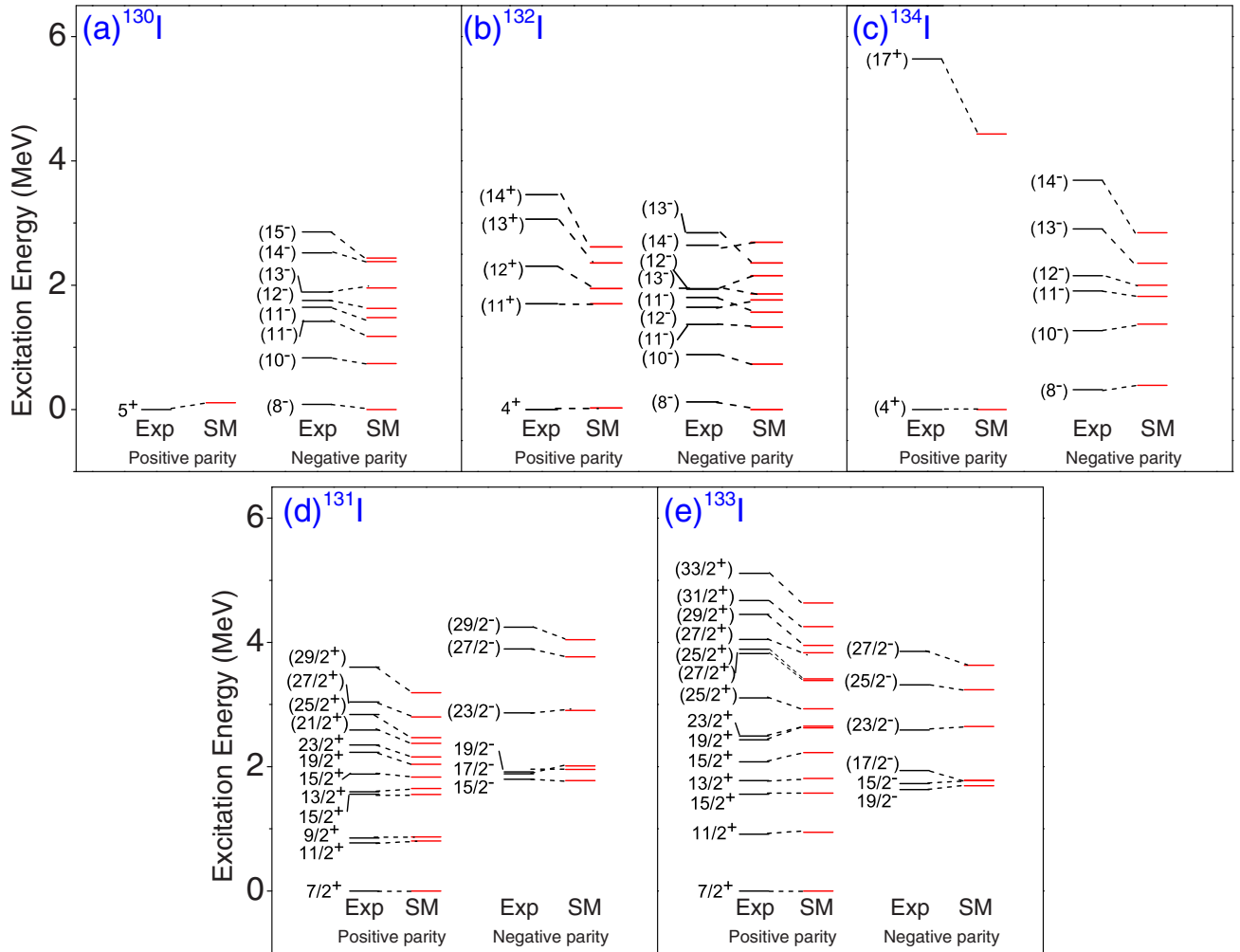


FIG. 16. The comparison of experimental (Exp, shown in black) and theoretical (SM, shown in red) level schemes for even- A $^{130,132,134}\text{I}$ (a)–(c) and odd- A $^{131,133}\text{I}$ (d)–(e) isotopes for both positive and negative parities. The experimental and shell model states of the same spin-parity have been joined with dotted lines to guide the eye.

understood as resulting from one proton excitation to the $\pi h_{11/2}$ orbital, leading to a $\pi g_{7/2}^2 \pi h_{11/2}$ configuration. The strongest decay of these states to the positive parity states is of $E3$ nature, corresponding to the $\pi h_{11/2} \rightarrow \pi d_{5/2}$ stretched $E3$ transition. An analogous pattern can be also observed in ^{134}Te [19,52]. From the results of the shell model calculations, in ^{135}I the $17/2^+$ and $19/2^-$, $21/2^-$, $23/2^-$ states are (not shown) between 200 and 400 keV lower as compared to the experimental values. In ^{134}I , the model calculations further under predict the excitation energy of the 13^- , 14^- , and 17^+ states [Fig. 16(c)].

For the odd- A iodine isotopes, $^{131,133}\text{I}$, the previously known positive parity states below the $23/2^+$, $19/2^-$, and $15/2^-$ isomers have been reproduced well in the present shell model calculations [Figs. 16(d)–16(e)]. The excited states above the $19/2^-$ isomer, in both $^{131,133}\text{I}$, are reported for the first time in the present work. The three levels above $19/2^-$ are assigned as $(23/2^-)$, $(27/2^-)$, and $(29/2^-)$ in ^{131}I and as $(23/2^-)$, $(25/2^-)$, and $(27/2^-)$ in ^{133}I , based on the agreement of the experimental results with the shell model calculation.

The level at 1938 keV in ^{133}I is newly observed in the current work and is connected to $15/2^+$ level via 378 keV transition. This state is assigned as $(17/2^-)$, following a similar assignment of a level reported earlier in ^{131}I [17].

We will now focus on the features of the negative parity states, $(8^-–14^-)$ in $^{130,132}\text{I}$ and $(19/2^-–31/2^-)$ in $^{131,133}\text{I}$. The present shell model calculations show that the proton particles in the $\pi g_{7/2}$, $\pi d_{5/2}$, $\pi h_{11/2}$ and neutron holes in the $\nu d_{3/2}$, $\nu s_{1/2}$, $\nu h_{11/2}$ have a leading contribution to the structure of the negative parity excited states. All the other orbitals remain relatively inactive. This work shows that, in case of $^{130–133}\text{I}$, the neutron hole occupancy in the $\nu h_{11/2}$ orbital can undergo variation as a function of the spin of the state, but, as can be seen in ^{134}I [18,51], all the states with the relevant spins could be made with only one neutron hole in the $\nu h_{11/2}$. In Figs. 17(a) and 18(a) the probability of neutron hole occupancy in the $\nu h_{11/2}$ orbital is shown as a function of the total spin (J) and ($2J$) of the negative parity states, for $^{130,132}\text{I}$ and $^{131,133}\text{I}$, respectively. It can be seen from the figures that

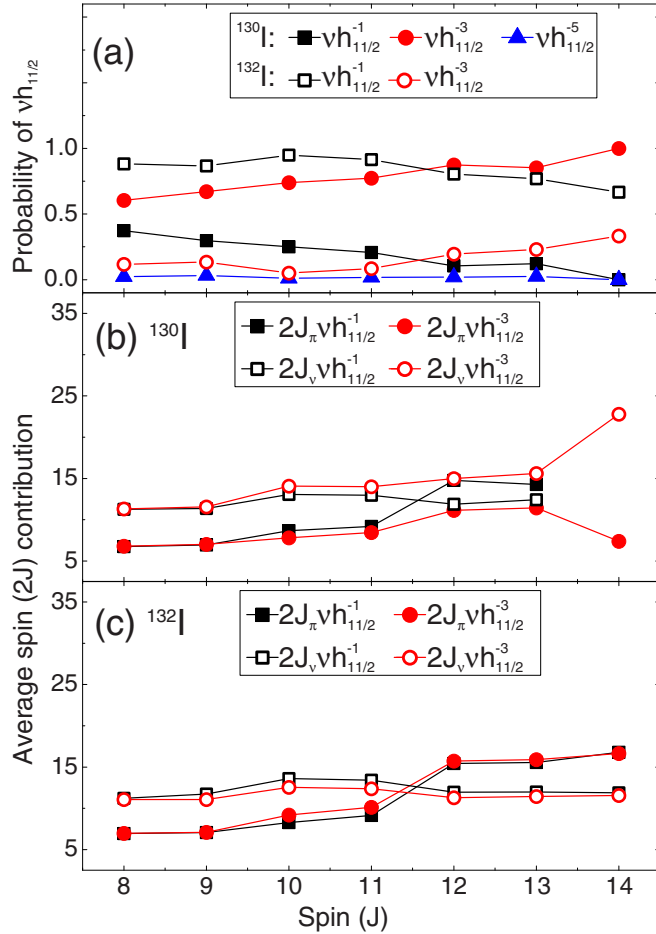


FIG. 17. (a) Probability of neutron hole occupancy in the $\nu h_{11/2}$ orbital for $^{130,132}\text{I}$ as a function of the total spin (J) of the negative parity states. (b) Average spin contributions of proton ($2J_\pi$) and neutron ($2J_\nu$) to the total spin (J) of the negative parity states in ^{130}I for different numbers of hole occupancy in the $\nu h_{11/2}$ orbital. (c) Same as (b), but for ^{132}I .

^{132}I : (three neutron holes) the main contribution is from the $\nu h_{11/2}^{-1}$, which slightly decreases at higher spin in favor of the $\nu h_{11/2}^{-3}$ configuration;

^{130}I : (five neutron holes) there is a large contribution of $\nu h_{11/2}^{-1}$ and $\nu h_{11/2}^{-3}$ at lower spin, while the $\nu h_{11/2}^{-3}$ dominates at higher spin, and the contribution of $\nu h_{11/2}^{-5}$ is negligible;

^{133}I : (two neutron holes) the $\nu h_{11/2}^{-1}$ configuration is almost pure;

^{131}I : (four neutron holes) the $\nu h_{11/2}^{-1}$ configuration dominates until $25/2^-$, beyond which the $\nu h_{11/2}^{-2}$ takes over, implying the contribution of the proton $\pi h_{11/2}$ excitation.

The average spin contributions of proton ($2J_\pi$) and neutron ($2J_\nu$) to the total spin of the negative parity states, for the configurations involving different occupancy of the $\nu h_{11/2}$ orbital, are shown in Fig. 17(b) for ^{130}I , Fig. 17(c) for ^{132}I , Fig. 18(b) for ^{131}I , and Fig. 18(c) for ^{133}I . In ^{132}I , at low spin,

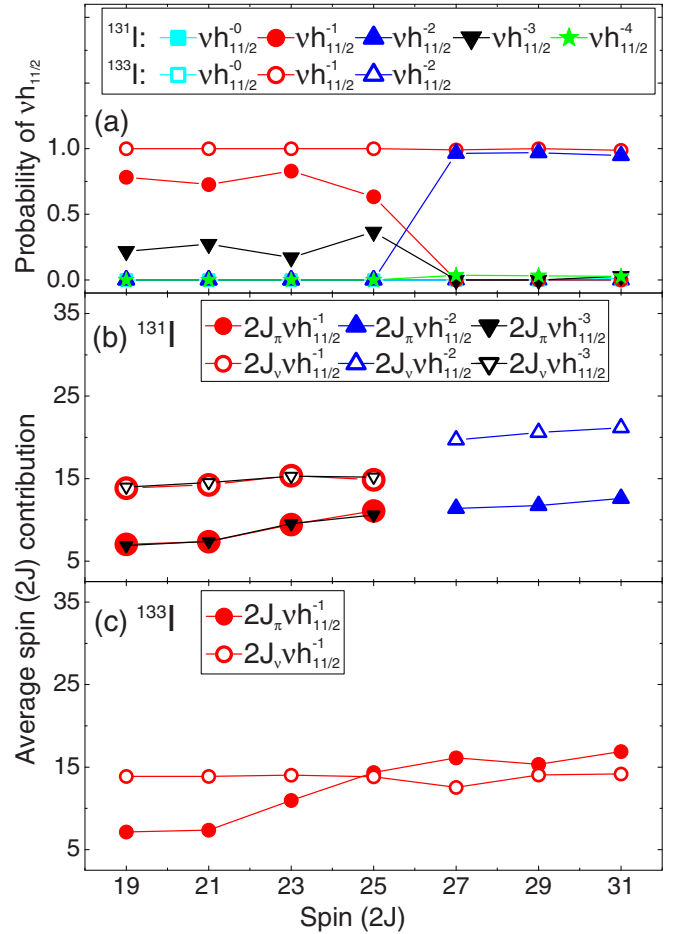


FIG. 18. (a) Probability of neutron hole occupancy in the $\nu h_{11/2}$ orbital for $^{131,133}\text{I}$ as a function of the total spin ($2J$) of the negative parity states. (b) Average spin contributions of proton ($2J_\pi$) and neutron ($2J_\nu$) to the total spin ($2J$) of the negative parity states in ^{131}I for different numbers of hole occupancy in the $\nu h_{11/2}$ orbital. (c) Same as (b), but for ^{133}I .

the average J_π^π is $7/2^+$ and J_ν^π is $11/2^-$. With increasing spin J , the average neutron spin remains almost constant, while the proton spin gradually increases towards the full spin alignment ($17/2^+$) of the three protons in the $\pi g_{7/2}$ and $\pi d_{5/2}$ orbitals, i.e., $|(\pi g_{7/2}^2; 6^+) \times (\pi d_{5/2}; 5/2^+); 17/2^+$. A similar behavior is also observed in ^{134}I (not shown), where the spin contribution of the single neutron hole in $\nu h_{11/2}$ is $11/2^-$. The average spin contributions for the dominant ($\nu h_{11/2}^{-1}$) configuration and for the admixture ($\nu h_{11/2}^{-3}$) closely follow each other. In ^{130}I , the trends are similar for the admixture ($\nu h_{11/2}^{-1}$), which has only a negligible contribution to the 14^- state. For the leading component ($\nu h_{11/2}^{-3}$), the proton spin contribution is smaller, which is compensated by the corresponding increase of the spin of the neutrons. In ^{133}I , at low spin, the average J_π^π is $7/2^+$ and J_ν^π is 7^- . The configuration of the $J_\nu^\pi = 7^-$ corresponds to the $\nu d_{3/2}^{-1} \nu h_{11/2}^{-1}$. With the increase of the final spin J , similarly to ^{132}I , the average neutron spin remains almost constant while the proton spin gradually increases towards the full spin alignment. In ^{131}I , the average spin contribution of

protons and neutrons below $25/2^-$ is similar to that observed for ^{133}I . The contributions from the dominant ($\nu h_{11/2}^{-1}$) configuration and the admixture ($\nu h_{11/2}^{-3}$) follow each other. The crossing between the average neutron and proton spin does not occur. At $27/2^-$, the configuration changes to $\nu h_{11/2}^{-2}$ and one proton is promoted to the $\pi h_{11/2}$ orbital. The average spin of protons J_{π}^{π} is $11/2^-$ and that of neutrons J_{ν}^{π} is 10^+ . The predicted, sudden change of the configuration involving the $\pi h_{11/2}$ excitation could, however, occur at too low excitation energy in the model, as already discussed earlier for ^{134}I . These shell model calculations for the negative parity states of $^{130-134}\text{I}$ in terms of their neutron and proton occupancies and spins were discussed. The importance of the hole occupancy of $\nu h_{11/2}$ orbital in generation of the high-spin negative parity states in these I isotopes was shown.

V. SUMMARY

The prompt-delayed spectroscopy of neutron-rich iodine isotopes $^{130-134}\text{I}$ was carried out after producing the nuclei in fusion-fission and transfer induced fission of the reaction $^9\text{Be}(^{238}\text{U}, f)$ at a beam energy of 6.2 MeV/u. The prompt transitions above the isomers in odd-odd $^{130,132}\text{I}$ were identified for the first time and a new isomer in ^{132}I is reported. The level scheme of ^{134}I is also extended. The high-spin level structures of $^{131,133}\text{I}$ were extended with the placement of new prompt transitions above the known isomers. The

proposed level schemes are interpreted in terms of systematics and large-scale shell model calculations. It is found that, the hole occupancy in the $\nu h_{11/2}$ orbital plays a dominant role in generating the high-spin negative parity states in these neutron-rich iodine isotopes. An additional feature, that the hole occupation of the $\nu h_{11/2}$ orbital varies strongly in certain I isotopes, could also be observed.

ACKNOWLEDGMENTS

The authors gratefully acknowledge the AGATA Collaboration for the availability of the AGATA γ tracking array at GANIL. We would like to thank the GANIL accelerator staff for their technical contributions. We thank A. O. Macchiavelli for help in data collection during the experiment. S.B., S.B., and R.B. acknowledge the support received from CEFIPRA Project No. 5604-4 and S.B. and R.P. acknowledge support from the LIA France-India agreement. P.B. and A.M. acknowledge support from the Polish National Science Centre (NCN) under Contract No. 2016/22/M/ST2/00269 and the French LEA COPIGAL project. H.L.C. and P.F. acknowledge support from the U.S. Department of Energy, Office of Science, Office of Nuclear Physics under Contract No. DE-AC02-05CH11231 (LBNL). R.M.P.-V. acknowledges partial support by the Ministry of Science, Spain, under the grants BES-2012-061407, SEV-2014-0398, and FPA2017-84756-C4, and by EU FEDER funds.

-
- [1] J. P. Schiffer and W. W. True, *Rev. Mod. Phys.* **48**, 191 (1976).
 [2] L. Coraggio, A. Covello, A. Gargano, N. Itaco, and T. T. S. Kuo, *Phys. Rev. C* **66**, 064311 (2002).
 [3] L. Coraggio *et al.*, *Nucl. Phys. A* **805**, 424 (2008).
 [4] B. Fogelberg, M. Hellstrom, D. Jerrestam, H. Mach, J. Blomqvist, A. Kerek, L.O. Norlin, and J. P. Omtvedt, *Phys. Rev. Lett.* **73**, 2413 (1994).
 [5] K. L. Jones *et al.*, *Nature (London)* **465**, 454 (2010).
 [6] M. Rejmund *et al.*, *Phys. Lett. B* **753**, 86 (2016).
 [7] S. Biswas, R. Palit, A. Navin, M. Rejmund, A. Bisoi, M. S. Sarkar, S. Sarkar, S. Bhattacharyya, D. C. Biswas, M. Caamano, M. P. Carpenter, D. Choudhury, E. Clement, L. S. Danu, O. Delaune, F. Farget, G. de France, S. S. Hota, B. Jacquot, A. Lemasson, S. Mukhopadhyay, V. Nanal, R. G. Pillay, S. Saha, J. Sethi, P. Singh, P. C. Srivastava, and S. K. Tandel, *Phys. Rev. C* **93**, 034324 (2016).
 [8] J. Genevey, J. A. Pinston, C. Foin, M. Rejmund, H. Faust, and B. Weiss, *Phys. Rev. C* **65**, 034322 (2002).
 [9] P. Bhattacharyya, P. J. Daly, C. T. Zhang, Z. W. Grabowski, S. K. Saha, R. Broda, B. Fornal, I. Ahmad, D. Seweryniak, I. Wiedenhover, M. P. Carpenter, R. V. F. Janssens, T.L. Khoo, T. Lauritsen, C. J. Lister, P. Reiter, and J. Blomqvist, *Phys. Rev. Lett.* **87**, 062502 (2001).
 [10] L. Coraggio, A. Covello, A. Gargano, and N. Itaco, *Phys. Rev. C* **87**, 034309 (2013).
 [11] H. Kaur, J. Singh, A. Sharma, J. Goswamy, D. Mehta, N. Singh, P. N. Trehan, E. S. Paul, and R. K. Bhowmik, *Phys. Rev. C* **55**, 512 (1997).
 [12] H. Kaur *et al.*, *Phys. Rev. C* **55**, 2234 (1997).
 [13] B. Kanagalekar, P. Das, B. Bhujiang, S. Muralithar, R. P. Singh, and R. K. Bhowmik, *Phys. Rev. C* **88**, 054306 (2013).
 [14] B. Ding, H. X. Wang, H. Jiang, Y. H. Zhang, X. H. Zhou, Y. M. Zhao, S. T. Wang, M. L. Liu, G. S. Li, Y. Zheng, N. T. Zhang, H. B. Zhou, Y. J. Ma, Y. Sasakiz, K. Yamada, H. Ohshima, S. Yokose, M. Ishizuka, T. Komatsubara, and K. Furuno, *Phys. Rev. C* **86**, 034302 (2012).
 [15] B. Ding, Y. H. Zhang, X. H. Zhou, G. X. Dong, F. R. Xu, M.L. Liu, G. S. Li, N. T. Zhang, H. X. Wang, H. B. Zhou, Y. J. Ma, Y. Sasakiz, K. Yamada, H. Ohshima, S. Yokose, M. Ishizuka, T. Komatsubara, and K. Furuno, *Phys. Rev. C* **85**, 044306 (2012).
 [16] D. Deleanu, D.L. Balabanski, T. Venkova, D. Bucurescu, N. Marginean, E. Ganioglu, G. Cata-Danil, L. Atanasova, I. Cata-Danil, P. Detistov, D. Filipescu, D. Ghita, T. Glodariu, M. Ivascu, R. Marginean, C. Mihai, A. Negret, S. Pascu, T. Sava, L. Stroe, G. Suliman, and N. V. Zamfir, *Phys. Rev. C* **87**, 014329 (2013).
 [17] H. Watanabe, G. J. Lane, G. D. Dracoulis, A. P. Byrne, P. Nieminen, F. G. Kondev, K. Ogawa, M. P. Carpenter, R. V. F. Janssens, T. Lauritsen, D. Seweryniak, S. Zhu, and P. Chowdhury, *Phys. Rev. C* **79**, 064311 (2009).
 [18] S. H. Liu, J. H. Hamilton, A. V. Ramayya, J. K. Hwang, A. V. Daniel, G. M. Ter-Akopian, Y. X. Luo, J. O. Rasmussen, S. J. Zhu, and W.C. Ma, *Phys. Rev. C* **79**, 067303 (2009).
 [19] S. K. Saha *et al.*, *Phys. Rev. C* **65**, 017302 (2001).
 [20] W. Urban *et al.*, *Eur. Phys. J. A* **27**, 257 (2006).
 [21] T. Rzaqca-Urban *et al.*, *Phys. Rev. C* **75**, 054319 (2007).
 [22] A. Korgul *et al.*, *Eur. Phys. J. A* **12**, 129 (2001).

- [23] W. Urban *et al.*, *Phys. Rev. C* **65**, 024307 (2002).
- [24] A. Navin *et al.*, *Phys. Lett. B* **728**, 136 (2014).
- [25] M. Rejmund *et al.*, *Nucl. Instrum. Methods Phys. Res. A* **646**, 184 (2011).
- [26] A. Navin and M. Rejmund, Gamma-ray spectroscopy of neutron-rich fission fragments, in *Yearbook of Encyclopedia of Science and Technology* (McGraw-Hill, New York, 2014).
- [27] M. Vandebrouck *et al.*, *Nucl. Instrum. Methods Phys. Res. A* **812**, 112 (2016).
- [28] Y. H. Kim *et al.*, *Eur. Phys. J. A* **53**, 162 (2017).
- [29] S. Akkoyun *et al.*, *Nucl. Instrum. Methods Phys. Res. A* **668**, 26 (2012).
- [30] J. Simpson *et al.*, *Act. Phys. Hung. Ser. Heavy Ion Phys.* **11**, 159 (2000).
- [31] S. Biswas *et al.*, *Phys. Rev. C* **99**, 064302 (2019).
- [32] S. L. Sakharov *et al.*, *Nucl. Phys. A* **494**, 36 (1989).
- [33] P. Puppe, A. Lennarz, T. Adachi, H. Akimune, H. Ejiri, D. Frekers, H. Fujita, Y. Fujita, M. Fujiwara, E. Ganioglu, E.W. Grewe, K. Hatanaka, R. Hodak, C. Iwamoto, N. T. Khai, A. Okamoto, H. Okamura, P. P. Povinec, G. Susoy, T. Suzuki, A. Tamii, J.H. Thies, and M. Yosoi, *Phys. Rev. C* **86**, 044603 (2012).
- [34] B. Singh, *Nucl. Data Sheets* **93**, 33 (2001).
- [35] S. V. Jackson *et al.*, *Phys. Rev. C* **11**, 1323 (1975).
- [36] G. Lhersonneau *et al.*, *Phys. Rev. C* **12**, 609 (1975).
- [37] E. S. Macias and W. B. Walters, *Nucl. Phys. A* **161**, 471 (1971).
- [38] R. L. Auble *et al.*, *Phys. Rev.* **169**, 955 (1968).
- [39] M. Dikić *et al.*, *Phys. Rev. C* **10**, 1172 (1974).
- [40] S. K. Das *et al.*, *Eur. Phys. J. A* **4**, 1 (1999).
- [41] S. Bhattacharyya *et al.*, *EPJ Web Conf.* **66**, 02009 (2014).
- [42] M. Tanigaki, S. Izumi, H. Ouchi, A. Sasaki, Y. Miyashita, N. Sato, S. Hoshino, K. Shimada, T. Wakui, T. Shinozuka, and Y. Ohkubo, *Phys. Rev. C* **80**, 034304 (2009).
- [43] H.G. Hicks, J. H. Landrum, E.A. Henry, R.A. Meyer, S. Brandt, and V. Paar, *Phys. Rev. C* **27**, 2203 (1983).
- [44] W. B. Walters, E. A. Henry, and R. A. Meyer, *Phys. Rev. C* **29**, 991 (1984).
- [45] R. A. Meyer *et al.*, *Phys. Rev. C* **13**, 1617 (1976).
- [46] V. Berg and A. Höglund, *Nucl. Phys. A* **175**, 495 (1971).
- [47] A. A. Sonzogni, *Nucl. Data Sheets* **103**, 1 (2004).
- [48] C. D. Coryell *et al.*, *Nucl. Phys. A* **179**, 689 (1972).
- [49] B. Brown and W. Rae, *Nucl. Data Sheets* **120**, 115 (2014).
- [50] B. A. Brown, N. J. Stone, J. R. Stone, I. S. Towner, and M. Hjorth-Jensen, *Phys. Rev. C* **71**, 044317 (2005).
- [51] L. Coraggio, A. Covello, A. Gargano, and N. Itaco, *Phys. Rev. C* **80**, 061303(R) (2009).
- [52] C. T. Zhang *et al.*, *Phys. Rev. Lett.* **77**, 3743 (1996).